JACS
JOURNAL OF THE AMERICAN CHEMICAL SOCIETY
Article
pubs.acs.org/JACS

Pivotal Role and Regulation of Proton Transfer in Water Oxidation on Hematite Photoanodes

Yuchao Zhang, Hongna Zhang, Hongwei Ji, Wanhong Ma, Chuncheng Chen,* and Jincai Zhao*

Key Laboratory of Photochemistry, Beijing National Laboratory for Molecular Sciences, Institute of Chemistry, Chinese Academy of Sciences, Beijing 100190, China

Supporting Information

ABSTRACT: Hematite is a promising material for solar water splitting; however, high efficiency remains elusive because of the kinetic limitations of interfacial charge transfer. Here, we demonstrate the pivotal role of proton transfer in water oxidation on hematite photoanodes using photoelectrochemical (PEC) characterization, the H/D kinetic isotope effect (KIE), and electrochemical impedance spectroscopy (EIS). We observed a concerted proton−electron transfer (CPET) characteristic for the rate-determining interfacial hole transfer, where electron transfer (ET) from molecular water to a surface-trapped hole was accompanied by proton transfer (PT) to a solvent water molecule, demonstrating a substantial KIE (~3.5). The temperature dependency of KIE revealed a highly flexible proton transfer channel along the hydrogen bond at the hematite/electrolyte interface. A mechanistic transition in the rate-determining step from CPET to ET occurred after OH^- became the dominant hole acceptor. We further modified the proton−electron transfer sequence with appropriate proton acceptors (buffer bases) and achieved a greater than 4-fold increase in the PEC water oxidation efficiency on a hematite photoanode.

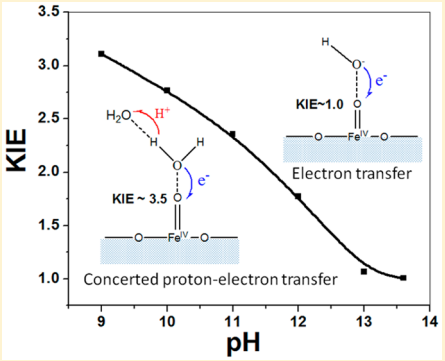

INTRODUCTION

Photoelectrochemical (PEC) water splitting is one of the most important strategies to store solar energy in chemical bonds. In this approach, water oxidation at photoanodes composed of metal oxides such as TiO_2,[1] WO_3,[2] and α-Fe_2O_3 (hematite)[3] is considered to be the major bottleneck limiting a system's efficiency. Hematite is a promising photoanode material for PEC water oxidation because of its desirable optical band gap (1.9−2.2 eV), high natural abundance, and good stability.[3] However, despite intensive efforts to improve the PEC activity of hematite by nanostructure engineering,[4,5] doping,[6−8] or surface modification,[9] the solar-to-hydrogen (STH) conversion efficiency of hematite electrodes remains far below the theoretical limit.[3]

The sluggish water oxidation kinetics on the surface of hematite is known to be a major efficiency-limiting factor. The mechanistic details for the associated elemental steps are poorly understood. The challenge lies in the complexity of the coupled $4e^-/4H^+$ processes, particularly the simultaneous potential/pH-determined interfacial reaction pathways in the rate-determining step (RDS). A thorough understanding of the underlying mechanism for this proton-coupled interfacial electron transfer process is of vital importance for obtaining efficient water splitting by engineering the surface to accelerate the sluggish kinetics.

Protonation equilibrium of the hematite surface has been investigated to gain mechanistic insight into the water oxidation properties of hematite. The stability of protonated vs deprotonated surface states has been hypothesized to determine both the thermodynamics of surface hole trapping, which is the first step in water oxidation on hematite, and the hematite water oxidation activity.[10−12] The literature contains evidence that the protonated surface states lead to quasi-Fermi-level pinning and that only deprotonated surface states have sufficient energy to initiate water oxidation.[13,14] The results of these previous studies on the effect of protonation equilibria on hole transfer suggest that the proton transfer could play an important role in water oxidation on the surface of hematite by controlling the thermodynamics of surface protonation/deprotonation. However, the significance of the kinetics of the associated proton transfer in water oxidation on hematite remains largely unexplored.

In this work, we exploit the H/D kinetic isotope effect to obtain direct information about the proton transfer kinetics and use electrochemical impedance spectroscopy (EIS), which is capable of distinguishing the process of hole trapping by surface states from that of the interfacial hole transfer to acceptors, to demonstrate that the surface hole transfer to a water molecule occurs via a concerted proton−electron transfer (CPET) pathway. To the best of our knowledge, this work represents the first direct evidence for a CPET pathway for the interfacial hole transfer from hematite surface states to water, although such a mechanism has been proposed for homogeneous water oxidation by molecular catalysis.[15−21] Inspired by these findings, we further regulate the proton transfer process using

Received: November 18, 2015
Published: February 9, 2016

DOI: 10.1021/jacs.5b12069
J. Am. Chem. Soc. 2016, 138, 2705−2711

buffer bases such as borate to improve the water oxidation activity of hematite photoanodes at near-neutral pH levels (pH 7−11).

RESULTS AND DISCUSSION

The J−V profiles of the hematite photoanode under AM 1.5G irradiation in unbuffered electrolytes (Figure 1) show three

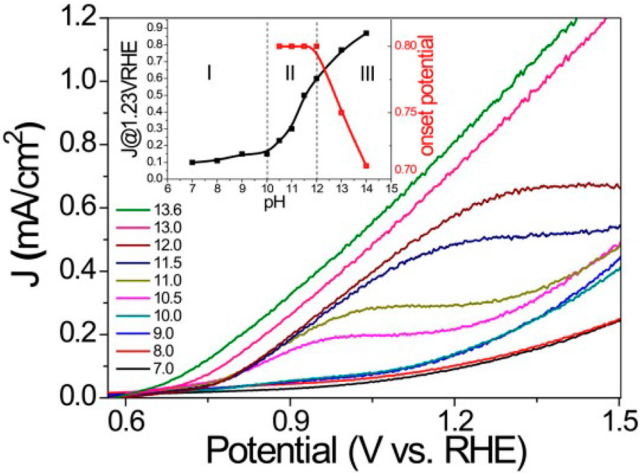

Figure 1. J−V scans (50 mV/s) under AM 1.5G illumination in unbuffered electrolytes (0.5 M $NaClO_4$) at different pH levels. The inset shows the photocurrent densities at 1.23 V_{RHE} and the onset potentials at different pH levels. (The onset potential below pH 10.5 is not shown because an accurate determination was not possible at the low photocurrent level.)

distinct pH regimes (Figure 1, inset): From pH 7 to pH 10, the activities are very poor, with photocurrent densities less than 0.16 mA cm^{-2} at 1.23 V_{RHE}. Above pH 12, the onset potential decreases with increasing pH in a Nernstian fashion (approximately 59 mV/pH), whereas the photocurrent density continues to increase. Intriguingly, an evident transition regime was observed between pH 10 and pH 12. In this regime, the onset potentials were approximately 0.8 V_{RHE} and remained unchanged, whereas the photocurrent increased gradually with increasing pH. The pK_a of the singly coordinated oxygen atoms on the surface of hematite (Fe^{III}−OH) has been reported to be approximately 10.[22−24] Around this pH, the interfacial protonation/deprotonation equilibrium shifts the valence band edge of hematite by 59 mV/pH vs NHE.[25] The behavior of the onset potential in this regime is consistent with proton-coupled surface hole trapping to give the same pH dependency as the valence-band potential.[10,11,26] Above pH 12, the surface is fully deprotonated, with no proton loss associated with the hole-trapping step and with the onset potential shifted by 59 mV/pH on the RHE scale.

Notably, photocurrent plateaus appeared between pH 10.5 and pH 12, and the plateau potential shifted anodically with increasing pH. In the electrolyte, the OH^- and H_2O are the only species that can be oxidized by holes. The oxidation of OH^- is known to be more energetically favorable than the oxidation of molecular water (E_{O_2/OH^-} = 0.401 V and E_{O_2/H_2O} = 1.229 V vs RHE[27]). At low potentials, oxidation of OH^- should dominate the faradic current, whereas the oxidation of H_2O is thermodynamically hindered. At higher pH, a higher applied potential is required for significant OH^- depletion, which corresponds to an anodic shift in plateau potential (the plateau was not observed at pH 13 and 13.6 below 1.5 V_{RHE} with sufficient OH^-). It is, however, difficult to explain the J−V feature of the presence of the plateau and its anodic shift just by oxidation of OH^- at pH < 12. The consumption of OH^- would lead to its depletion on the electrode. If OH^- oxidation is the only reaction, a "pseudopeak" (a decrease in dJ/dV, as in cyclic voltammetry under the condition of competitive substrate consumption and diffusion), instead of a plateau, would be expected. The presence of a photocurrent plateau in our experiments (Figure 1) suggests oxidation of additional species to sustain the photocurrent after OH^- is depleted at high potentials. It is the competitive oxidation of this species and OH^- that is responsible for the appearance of the plateau. Naturally, the dominant hole acceptor after the plateau is assigned to the other oxidable reagent H_2O in the electrolyte, since the oxidation of molecular H_2O would become thermodynamically favorable at high potentials. The continuous photocurrent increase after the plateaus (at high potential, pH 10.5−11) is an indication that the solvent water molecule is the dominant reactant in this region, because the concentration of the solvent molecule is not limited by diffusion and its oxidation on the electrode would lead to continuously increased current until it is limited by the amount of photogenerated holes.[28]

The switch from OH^- to H_2O as the dominant hole acceptor was further confirmed by the photocurrent transients (I−t curves) at constant applied potentials (see the details in the Supporting Information, Figure S1). Briefly, I−t profiles exhibited an initial rapid decay, which is a typical feature of electron and surface-trapped hole recombination,[29] and a slow decay below pH 12 due to the depletion of OH^- and the release of the proton. Interestingly, the latter was most prominent at plateau potentials, consistent with the switch from OH^- to H_2O as the dominant hole acceptor. The slow photocurrent decays became less remarkable after the plateau potentials, which suggests that the diffusion of OH^- and proton does not limit the photocurrent anymore under high applied potentials, further supporting that the solvent water is oxidized at high potentials. In the presence of sufficient OH^- (pH > 12), oxidation of OH^- dominated the photocurrent, with no slow decay observed below 1.5 V_{RHE} (Figure S1).

To gain insight into the role of proton transfer in the water oxidation elemental steps, we first compared the PEC water oxidation in H_2O and D_2O at various pH/pD values (pD = pH_{read} + 0.4) and applied potentials. To avoid complications from surface hole trapping (nonfaradic current), the steady-state photocurrent from the I−t curves at each potential after 60 s of irradiation was used to calculate the kinetic isotope effect (KIE = $I(H_2O)/I(D_2O)$). As shown in Figure 2A, for all tested potentials, pronounced KIEs were observed at lower pH values (9−11), whereas the KIE value dropped to 1.5−1.7 at pH 12.0 and became nearly unity at pH 13.0 and 13.6. The KIE was potential-dependent, with higher values being obtained at more positive potentials. For example, the KIE increased from 2.0 to 3.1 with applied potentials of 1.0−1.2 V at pH 9.0. Because oxidation of molecular H_2O is the dominant reaction at low pH and high potentials, as noted in the discussion of Figure 1 and Figure S1, a large KIE is correlated to the oxidation of H_2O, indicating that the cleavage of the O−H bonds of water molecules is involved in RDS of water oxidation. It proceeds through a concerted proton−electron transfer (CPET) pathway; i.e., the electron transfer occurs simultaneously with the proton transfer to break the O−H

DOI: 10.1021/jacs.5b12069
J. Am. Chem. Soc. 2016, 138, 2705−2711

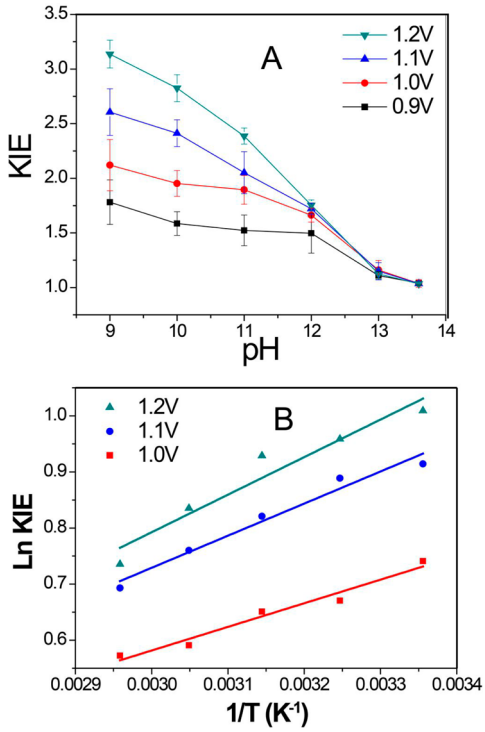

Figure 2. (A) KIE values calculated from the steady photocurrent ratio in H_2O and D_2O for a hematite photoanode in unbuffered electrolyte at various electrolyte pH levels and potentials and under LED illumination with λ = 470 nm and I_0 = 216 mW/cm^2. (B) Arrhenius plots of the temperature-dependent KIE performed at pH 10.0 between 1.0 and 1.2 V_{RHE}, ranging from 298 to 338 K.

bond. Such a mechanism is adopted in homogeneous catalysis[15−21] and biological systems[16] for water oxidation because of its thermodynamic advantage of avoiding the high-energy intermediates. At high pH or at low potentials, much lower KIE values were observed, reaching 1.0 at pH 13.6, which suggests that electron transfer is the dominant pathway in OH^- oxidation.

As the water dissociation constant is smaller in D_2O than in H_2O,[30] the concentration of OD^- is 7.5 times smaller than that of OH^- when $[H^+] = [D^+]$. To exclude the possibility that the pronounced KIE in the proposed H_2O oxidation region originates from the concentration difference of OH^- in H_2O and D_2O (the so-called concentration isotope effect),[31] we compared the photocurrent between H_2O and D_2O systems at the same concentrations of OH^- and OD^-. Pronounced "KIE" values were again observed at low pH values, and exhibited a tendency similar to that at $[H^+] = [D^+]$ (Figure S2). These observations confirm that the pronounced KIE is the intrinsic feature of oxidation of molecular H_2O. It is also notable that "KIE" values for $[OH^-] = [OD^-]$ were lower than those measured in the $[H^+] = [D^+]$ situation, which suggests that the concentration difference of OH^- in H_2O and D_2O could contribute moderately to the KIEs measured at $[H^+] = [D^+]$.

To gain a deeper insight into proton transfer in the CPET step, the temperature dependency of KIE was investigated at pH 10.0 between 1.0 V_{RHE} and 1.2 V_{RHE}, ranging from 298 to 338 K, as shown in Figure 2B and Figure S3. The calculated activation energy and pre-exponential factors are listed in Table 1. For all tested potentials, the observed KIE values decreased with the elevated temperatures (Figure S3A). The activation energy (E_a) was quite insensitive to the applied potentials, in

Table 1. Activation Energy and Pre-Exponential Factors Calculated from Arrhenius Plots at Different Potentials (vs RHE)

	1.0 V		1.1 V		1.2 V	
	H_2O	D_2O	H_2O	D_2O	H_2O	D_2O
E_a(kJ/mol)	12.8	16.3	13.4	18.2	13.2	18.7
A	0.033	0.066	0.053	0.142	0.054	0.183
A_H/A_D	0.50		0.37		0.30	
ΔE_a (kJ/mol)	3.5		4.8		5.5	

agreement with the previous reports for PEC water oxidation on hematite.[32] The fitted E_a in D_2O was pronouncedly larger than that in H_2O, and the ΔE_a became more prominent at positive potentials (ΔE_a = 3.5 kJ/mol at 1.0 V_{RHE} to 5.5 kJ/mol at 1.2 V_{RHE}). It is interesting to find that the pre-exponential factors in H_2O were much smaller than that in D_2O ($A_H/A_D \ll 1$). In addition, the ratios were reduced with the increased potentials (from 0.50 at 1.0 V_{RHE} to 0.30 at 1.2 V_{RHE}). Such differences in the Arrhenius parameters ($A_H/A_D \ll 1$ and large ΔE_a) between D_2O and H_2O suggest that the proton transfer occurs in a very flexible environment,[33−37] as discussed below.

It has been well accepted that water oxidation on hematite is mediated by surface-trapped holes,[10,13] which means that photogenerated holes are first trapped by surface iron species (most likely $\equiv Fe^{III}OH$) and then further react with surface-adsorbed H_2O/OH^-. KIE obtained from the photocurrent provides overall information about the significance of proton transfer in water oxidation reaction kinetics. To differentiate the role of proton transfer in surface hole trapping and in the subsequent hole transfer steps, EIS experiments were performed for unbuffered electrolyte in H_2O and D_2O at pH/pD = 10.0. The Nyquist plots exhibited two semicircles (Figure 3 and Figure S5) at 1.23 V_{RHE}, consistent with water

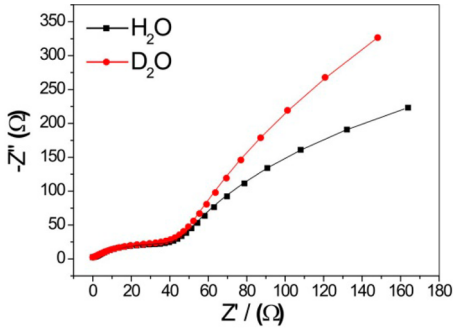

Figure 3. Nyquist plots for EIS conducted in H_2O and D_2O for a hematite photoanode at 1.23 V_{RHE} in an unbuffered electrolyte at pH/pD 10.0.

oxidation on a hematite photoanode occurring through the holes accumulated at the surface states.[10,12,13] The high-frequency semicircle, which represents the process of hole trapping by the surface states (hole accumulation at the surface),[13,38] was almost the same for the photoanode in H_2O and D_2O. However, the radius of the low-frequency semicircle, which reflects the process of the interfacial hole transfer to water,[9,10] was much smaller for the photoanode in H_2O than in D_2O. The parameters of charge transfer kinetics were fitted from the Nyquist plots using the equivalent circuit in Figure S4.[13,38] As shown in Table 2, the fitted $R_{trapping}$ (resistance in surface hole trapping) and C_{trap} (charges accumulated at surface

DOI: 10.1021/jacs.5b12069
J. Am. Chem. Soc. 2016, 138, 2705−2711

Table 2. Fitted EIS Parameters and the Photocurrent Measured in Different Electrolytes[a]

	$R_{trapping}$ (Ω)	C_{trap} (μF)	$R_{ct,trap}$ (Ω)	photocurrent (mA)
H_2O	60.5	540	769	0.14
D_2O	66.2	398	2700	0.05
H_2O + buffer	69.8	1150	250	1.4
D_2O + buffer	66.3	1380	230	1.2

[a]Measured in unbuffered and borate-buffered electrolyte at pH/pD 10.0 and at 1.23 V_{RHE} under LED illumination with λ = 470 nm and I_0 = 216 mW/cm^2.

states) in H_2O and D_2O were consistently quite similar, excluding that the KIE is caused by the surface hole trapping. These results also exclude the possibility that the "equilibrium isotope effect" caused by the different adsorption/desorption equilibria of H/D on the hematite surface is responsible for the observed KIE. The adsorption/desorption equilibrium of H/D would change the surface-protonating state, which is reported to determine the hole-trapping process.[14] Since the hole-trapping process was not influenced by the replacement of H_2O with D_2O, the "equilibrium isotope effect" should not contribute much to the KIEs under the present conditions.

By contrast, $1/R_{ct,trap}$, which is used here to represent the feasibility of hole transfer to water, was substantially larger in H_2O than that in D_2O, corresponding to a KIE of 3.5, consistent with the value obtained from the photocurrent at 1.23 V_{RHE} (Table 2) during the EIS experiments. These results allow the assignment of the CPET mechanism to interfacial hole transfer, not surface hole trapping.

The proton transfer pathways for interfacial hole transfer under different conditions are summarized in Scheme 1. The

Scheme 1. Electron−Proton Transfer Pathways during Interfacial Hole Transfer for Oxidation of (a) H_2O and (b) OH^-

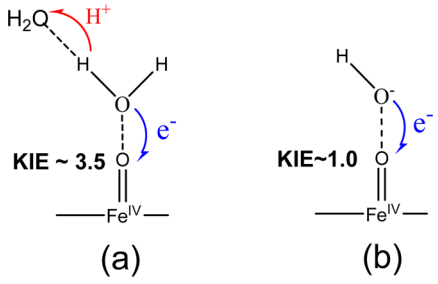

surface-trapped holes have been suggested to possess a chemical nature of high-valent Fe^{IV}=O species (sometimes referred to as a surface state with a particular energy level in the band gap).[10,13,39] Water oxidation involves four-electron loss (hole transfer) and four-proton release.[40,41] Although every hole transfer step involves a proton transfer in principle, the sequence of the electron−proton transfer in each step and its role in the whole water oxidation process are quite complex. In the present study, the large KIE values indicate that the RDS step proceeds according to a CPET mechanism. On the basis of the previous theoretical and experimental results on oxide-based water oxidation,[14,32,42] the RDS is tentatively assigned to the first hole transfer from the surface-trapping site to adsorbed H_2O, as shown in Scheme 1.

Our experiments revealed a potential/pH-dependent electron−proton transfer sequence in the RDS. Below pH 12 and at high potentials, transfer of the surface-trapped hole to the water molecules dominates the photocurrent. Under these conditions, the CPET pathway prevails (Scheme 1a), where an electron is transferred from H_2O to Fe^{IV}=O (surface hole) with concomitant proton transfer to break the O−H bond. At low pH values, the most likely proton acceptor is the solvent water molecule. Because water is an extremely poor proton acceptor (H_3O^+ pK_a = −1.7), the present work suggests that the absence of an appropriate proton acceptor in the interfacial hole transfer processes is largely responsible for the slow water oxidation kinetics and poor activity of hematite photoanodes at low pH. Notably, KIE values were nonunity even under quite low potentials, where the hole transfer to OH^- dominated the photocurrent, as shown in Figure 1 and Figure S1.

Two possible origins can be invoked to rationalize the moderate KIEs of 1.5−1.7 at low potentials: (1) Apart from oxidation of OH^-, oxidation of H_2O might occur and could contribute to the nonunity KIEs. (2) The moderate KIEs might also originate from the oxidation process of OH^- itself. If the first possibility is the case, the relative importance of the oxidation of OH^- and H_2O to the photocurrent and consequently the KIE values should be markedly condition-dependent. Our experiments showed that the KIEs at pH 12.0 under all tested potentials and at potential of 0.9 V_{RHE} between pH 9 and pH 12 remained approximately constant (1.5−1.7) (Figure 2A), thereby excluding the first possibility. The nonunity KIE at pH ≤ 12 at low potentials should be mainly due to the CPET-based oxidation of OH^-. Also, the concentration difference of OH^- in H_2O and D_2O could contribute partly to the observed KIEs, as mentioned above. At pH > 12, the unity KIEs at all applied potentials suggest an electron transfer (ET) as the dominant pathway; that is, the proton transfer is no longer involved in the rate-determining step. Under these conditions, the OH^- can act as a proton acceptor instead of the solvent water because of its high concentration. The high proton affinity of OH^- can decrease the magnitude of KIE, similar to the buffer effect discussed below. Notably, the mechanisms for the interfacial hole transfer for the formation of an O−O bond have been reported to proceed via either nucleophilic attack of Fe^{IV}=O by water or by the coupling of two adjacent Fe^{IV}=O species on the surface.[43] The KIE observed here supports the hypothesis of nucleophilic attack by a water molecule for the investigated hematite photoanode because the multiple Fe^{IV}=O coupling process does not involve proton transfer.

The temperature-dependent KIE experiments revealed a compelling feature of proton transfer in CPET at the hematite surface (Figure 2B and Table 1). Proton transfer is very sensitive to the potential energy barrier shape, which may be modulated by environmental oscillations of the reaction sites. The enhanced environmental oscillations would compress the proton transfer distance in the reaction coordinate and vice versa.[36,37] The significant temperature dependence of the KIE, $A_H/A_D \ll 1$ and large ΔE_a are the evident indications that the environment of the interfacial sites for the occurrence of the CPET reaction is quite "soft"; that is, the oscillation frequency of the environment is low enough to be thermally accessible. The temperature-dependent environment oscillation would change the distance for hydrogen transfer. Consequently, the hydrogen-tunneling probability can be modulated through the temperature. According to our mechanistic proposal (Scheme 1), the proton acceptor in the CPET process is the solvent water molecule. It is evident that this water molecule is located

DOI: 10.1021/jacs.5b12069
J. Am. Chem. Soc. 2016, 138, 2705−2711

in a very flexible environment formed by other water molecules through hydrogen bonds, which may rationalize the temperature-dependent characteristics of KIE. In addition, the changing tendency of higher ΔE_a and lower A_H/A_D at higher applied potentials (Table 1) suggests the softer environment of the reaction sites for the CPET on hematite at high potentials, where the oxidation of molecular H_2O is proposed to occur.

The aforementioned results suggest that the photoelectrochemical water oxidation on hematite under near-neutral conditions is limited kinetically by the proton transfer because of the poor proton-accepting property of solvent water. Fortunately, buffer bases, which have been used extensively to regulate the proton-coupled electron transfer process by facilitating proton transfer,[17,44,45] are promising for enhancement of the PEC water oxidation efficiency. As shown in Figure 4, greatly improved performance was observed upon addition of

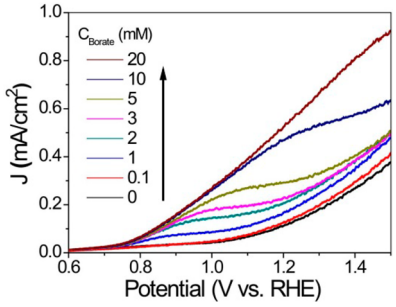

Figure 4. $J-V$ scans collected for a hematite photoanode with different concentrations of borate buffer solution at pH 10.0.

boric acid/borate buffer at pH 10.0. For example, the photocurrent density at 1.23 V_{RHE} increased from 0.13 mA/cm^2 in the unbuffered electrolyte to 0.57 mA/cm^2 (enhancement of over 4-fold) in the presence of 20 mM borate buffer, similar to the activity obtained at pH 12. Indeed, the introduction of other buffers, including $H_2PO_4^-/HPO_4^{2-}$, HCO_3^-/CO_3^{2-}, $H_3SiO_3/H_2SiO_3^-$, and $HTeO_3^-/TeO_3^{2-}$, also boosted the PEC efficiencies for water splitting in specific pH ranges (Figure S6). The photocurrent enhancement vs pH followed the titration curve of the buffer, rising sharply at the approximate pK_a of the buffer (Figure S7A). For example, the photocurrent enhancement in the presence of $H_3BO_3/H_2BO_3^-$ appeared at pH 8.5 and reached its maximum at pH 10.5 (the pK_a of boric acid is 9.24)[16] (Figure S7B). The correlation between the photocurrent enhancement's inflection and pK_a confirmed that only the base components are critical for improving the activity via accepting the proton from the O−H bond. Notably, the dependence of the $J-V$ profile on the buffer concentration (Figure 4) was similar to that observed for $J-V$ as the pH increases (Figure 1), including the photocurrent enhancement and the anodic shift of the photocurrent plateau potentials.

The role of the buffer base in proton transfer was further investigated by KIE measurements. Similar to the case of OH^-, the addition of borate greatly decreased the KIE value at all applied potentials (Figure S8). Such changes in the $J-V$ profile and KIE upon the addition of buffer suggest that the enhanced activity in the buffered electrolytes could originate from the increased local concentration of OH^-, because the buffer effects can maintain the OH^- concentration at the interface once it is consumed during oxidation. In addition, due to the higher basicity of buffer ions, the use of buffer would greatly accelerate the proton transfer kinetics during water oxidation, compared to the water molecules. This would also lead to a decrease in the KIE.[16] Therefore, the role of buffers in boosting the water oxidation is two-fold: the buffer (I) maintains the interfacial local concentration of the active species OH^- and (II) acts as a proton acceptor to accelerate the proton transfer.

Recently, Lee and co-workers reported that phosphate modification of the hematite surface can be a feasible strategy to mitigate charge recombination by extraction of photoexcited holes to the surface owing to the surface negative charge and realize a remarkable activity in a neutral electrolyte (potassium phosphate buffer).[46] Their EIS study also indicated that the interfacial charge transfer was greatly improved on the modified anode. Our EIS measurements revealed that buffer ions in neutral electrolyte could also facilitate the surface hole transfer to adsorbed H_2O at low pH by regulating the PCET step (Table 2). It is reasonable that the critical role of surface PCET proposed in the present study should work in Lee's system and contribute to the enhanced PEC activity in a neutral electrolyte.

CONCLUSION

Our study demonstrated that the rate-determining interfacial hole transfer to water molecules at the hematite surface is a concerted proton−electron transfer process at pH < 12, as evidenced by the significant H/D kinetic isotope effect arising from O−H bond cleavage upon proton transfer to solvent water. An important implication of our results is that the low activity under neutral conditions arises from proton transfer concomitant with the interfacial hole transfer due to the lack of an appropriate proton acceptor. This allows us to regulate the proton transfer kinetics and sequences by addition of buffer bases, achieving greatly enhanced PEC water oxidation activity by the buffer either maintaining the local interfacial OH^- concentration or acting as a proton acceptor. Our study highlights the significance of tuning interfacial proton transfer for improvement of solar water splitting with hematite photoanodes.

EXPERIMENTAL SECTION

Photoanode Preparation. Hematite nanowires were prepared on a fluorine-doped tin oxide (FTO; TCO-15, Nippon Sheet Glass, Japan, 14 Ω/sq) glass substrate by a modified procedure reported by Yat Li and co-workers.[7] Briefly, 100 mL of aqueous solution containing 2.43 g of ferric chloride ($FeCl_3 \cdot 6H_2O$; Alfa Aesar, 98%) and 0.85 g of sodium nitrate ($NaNO_3$; J&K, 99%) at pH 1.4 (adjusted by HCl) were prepared in a Teflon-lined stainless steel autoclave. Several FTO glass slides (2 × 4 cm), washed with acetone, ethanol, and then deionized water, were placed in the autoclave and heated at 95 °C for 4 h. After the hydrothermal treatment, a uniform layer of iron oxyhydroxide (FeOOH) was coated on the FTO glass, which was washed completely with deionized water to remove any residual salts. The obtained film was sintered in air at 550 °C for 2 h and at 750 °C for 15 min to convert FeOOH into hematite.

Photoelectrochemical Characterization. The PEC performances of the photoanodes were measured in a three-electrode electrochemical cell. The electrolyte solution was deaerated by purging argon for 30 min before the $J-V$ scan. The measured potentials vs Ag/AgCl were converted to the reversible hydrogen electrode (RHE) scale according to the Nernst equation: $E_{RHE} = E_{Ag/AgCl} + 0.059pH + 0.1976$. A 150 W xenon lamp coupled to a filter (AM 1.5G) was used as the light source. The light power density of 100 mW/cm^2 was measured with a radiometer (CEAULIGHT, CEL-NP2000). The $J-V$ scan rate was 50 mV/s. The transient $I-t$ experiments were performed under AM 1.5G illumination equipped with an electronic shutter. KIE and EIS experiments were measured under LED illumination (λ = 470

DOI: 10.1021/jacs.5b12069
J. Am. Chem. Soc. 2016, 138, 2705−2711

nm, I_0 = 216 mW/cm^2), recorded by an electrochemical workstation (PGSTAT302N autolab, Metrohm). For EIS measurement, a sinusoidal voltage pulse of 10 mV amplitude was applied on a bias voltage, with frequencies that ranged from 10 kHz to 1 Hz. The raw data were fitted and simulated using Nova 1.8 software from Metrohm Inc. For KIE experiments, D_2O (99.9%) was purchased from Cambridge Isotope Laboratories, Inc. The pH values of the solution were measured by a pH meter (Thermo Scientific, 3-Star). The pD values were obtained followed the relation pD = pH_{read} + 0.4. The pD values were adjusted by NaOD (Alfa Aesar, 40% (w/w) solution in D_2O, 99.5% (isotopic)) and D_2SO_4 (Alfa Aesar, 96% min in D_2O, 99.5% (isotopic)). All experiments were performed at a room temperature of 25 ± 3 °C unless otherwise noted. The KIE results were the averaged values from four experimental runs. For temperature-dependent KIE experiments, the temperature was controlled by a homemade thermostatic water bath device equipped with a matched water-recycled electrochemical cell. The LED illumination reaching the working electrode in this cell is 180 mW/cm^2. The effect of the temperature on the reference electrode was calibrated by the reported temperature-dependent standard potential of the Ag/AgCl electrode.[47]

■ ASSOCIATED CONTENT

Supporting Information

The Supporting Information is available free of charge on the ACS Publications website at DOI: 10.1021/jacs.5b12069.

Transient $I-t$ profile, comparison of KIE values, data from temperature effect experiments, Arrhenius plot of the photocurrent, model circuit for EIS fitting, Nyquist plots obtained during EIS measurements, $J-V$ scans collected in buffered solutions, titration pH for photocurrent enhancements as a function of the corresponding pK_a of the buffer, ratio of the photocurrent density between systems with and without boric acid, and KIE values collected for a hematite photoanode (PDF)

■ AUTHOR INFORMATION

Corresponding Authors

*ccchen@iccas.ac.cn

*jczhao@iccas.ac.cn

Notes

The authors declare no competing financial interest.

■ ACKNOWLEDGMENTS

We are grateful for the financial support of this work by the 973 project (Grant No. 2013CB632405), the National Natural Science Foundation of China (NSFC) (Grant Nos. 21590811, 21137004, 21525729, and 21221002), and the "Strategic Priority Research Program" of the Chinese Academy of Sciences (Grant No. XDA09030200).

■ REFERENCES

(1) Fujishima, A.; Honda, K. *Nature* **1972**, *238*, 37.

(2) Mi, Q.; Ping, Y.; Li, Y.; Cao, B.; Brunschwig, B. S.; Khalifah, P. G.; Galli, G. A.; Gray, H. B.; Lewis, N. S. *J. Am. Chem. Soc.* **2012**, *134*, 18318.

(3) Sivula, K.; Le Formal, F.; Gratzel, M. *ChemSusChem* **2011**, *4*, 432.

(4) Cesar, I.; Kay, A.; Martinez, J. A. G.; Gratzel, M. *J. Am. Chem. Soc.* **2006**, *128*, 4582.

(5) Tilley, S. D.; Cornuz, M.; Sivula, K.; Gratzel, M. *Angew. Chem., Int. Ed.* **2010**, *49*, 6405.

(6) Wang, G.; Ling, Y.; Wheeler, D. A.; George, K. E.; Horsley, K.; Heske, C.; Zhang, J. Z.; Li, Y. *Nano Lett.* **2011**, *11*, 3503.

(7) Ling, Y.; Wang, G.; Wheeler, D. A.; Zhang, J. Z.; Li, Y. *Nano Lett.* **2011**, *11*, 2119.

(8) Zhang, Y.; Jiang, S.; Song, W.; Zhou, P.; Ji, H.; Ma, W.; Hao, W.; Chen, C.; Zhao, J. *Energy Environ. Sci.* **2015**, *8*, 1231.

(9) Zhang, Y.; Zhou, Z.; Chen, C.; Che, Y.; Ji, H.; Ma, W.; Zhang, J.; Song, D.; Zhao, J. *ACS Appl. Mater. Interfaces* **2014**, *6*, 12844.

(10) Klahr, B.; Gimenez, S.; Fabregat-Santiago, F.; Bisquert, J.; Hamann, T. W. *Energy Environ. Sci.* **2012**, *5*, 7626.

(11) Haghighat, S.; Dawlaty, J. M. *J. Phys. Chem. C* **2015**, *119*, 6619.

(12) Upul Wijayantha, K. G.; Saremi-Yarahmadi, S.; Peter, L. M. *Phys. Chem. Chem. Phys.* **2011**, *13*, 5264.

(13) Klahr, B.; Gimenez, S.; Fabregat-Santiago, F.; Hamann, T.; Bisquert, J. *J. Am. Chem. Soc.* **2012**, *134*, 4294.

(14) Iandolo, B.; Hellman, A. *Angew. Chem., Int. Ed.* **2014**, *53*, 13404.

(15) Song, N.; Concepcion, J. J.; Binstead, R. A.; Rudd, J. A.; Vannucci, A. K.; Dares, C. J.; Coggins, M. K.; Meyer, T. J. *Proc. Natl. Acad. Sci. U. S. A.* **2015**, *112*, 4935.

(16) Weinberg, D. R.; Gagliardi, C. J.; Hull, J. F.; Murphy, C. F.; Kent, C. A.; Westlake, B. C.; Paul, A.; Ess, D. H.; McCafferty, D. G.; Meyer, T. J. *Chem. Rev.* **2012**, *112*, 4016.

(17) Irebo, T.; Reece, S. Y.; Sjodin, M.; Nocera, D. G.; Hammarstrom, L. *J. Am. Chem. Soc.* **2007**, *129*, 15462.

(18) Sjödin, M.; Styring, S.; Åkermark, B.; Sun, L.; Hammarström, L. *J. Am. Chem. Soc.* **2000**, *122*, 3932.

(19) Sjödin, M.; Styring, S.; Wolpher, H.; Xu, Y.; Sun, L.; Hammarström, L. *J. Am. Chem. Soc.* **2005**, *127*, 3855.

(20) Sjödin, M.; Irebo, T.; Utas, J. E.; Lind, J.; Merényi, G.; Åkermark, B.; Hammarström, L. *J. Am. Chem. Soc.* **2006**, *128*, 13076.

(21) Irebo, T.; Reece, S. Y.; Sjödin, M.; Nocera, D. G.; Hammarström, L. *J. Am. Chem. Soc.* **2007**, *129*, 15462.

(22) Chatman, S.; Zarzycki, P.; Preočanin, T.; Rosso, K. M. *J. Colloid Interface Sci.* **2013**, *391*, 125.

(23) Lützenkirchen, J.; Preočanin, T.; Stipić, F.; Heberling, F.; Rosenqvist, J.; Kallay, N. *Geochim. Cosmochim. Acta* **2013**, *120*, 479.

(24) Chatman, S.; Zarzycki, P.; Rosso, K. M. *Phys. Chem. Chem. Phys.* **2013**, *15*, 13911.

(25) Lin, Y.; Yuan, G.; Sheehan, S.; Zhou, S.; Wang, D. *Energy Environ. Sci.* **2011**, *4*, 4862.

(26) Hellman, A.; Pala, R. G. S. *J. Phys. Chem. C* **2011**, *115*, 12901.

(27) Bard, A. J. *J. Am. Chem. Soc.* **2010**, *132*, 7559.

(28) Savéant, J.-M. *Chem. Rev.* **2008**, *108*, 2348.

(29) Dotan, H.; Sivula, K.; Grätzel, M.; Rothschild, A.; Warren, S. C. *Energy Environ. Sci.* **2011**, *4*, 958.

(30) Bell, R. P. *The Proton in Chemistry*, 2nd ed.; Cornell University Press: New York, 1973.

(31) Irebo, T.; Zhang, M.-T.; Markle, T. F.; Scott, A. M.; Hammarström, L. *J. Am. Chem. Soc.* **2012**, *134*, 16247.

(32) Cowan, A. J.; Barnett, C. J.; Pendlebury, S. R.; Barroso, M.; Sivula, K.; Gratzel, M.; Durrant, J. R.; Klug, D. R. *J. Am. Chem. Soc.* **2011**, *133*, 10134.

(33) Bell, R. P. *Chem. Soc. Rev.* **1974**, *3*, 513.

(34) Kwart, H. *Acc. Chem. Res.* **1982**, *15*, 401.

(35) Bonin, J.; Costentin, C.; Louault, C.; Robert, M.; Savéant, J.-M. *J. Am. Chem. Soc.* **2011**, *133*, 6668.

(36) Knapp, M. J.; Rickert, K.; Klinman, J. P. *J. Am. Chem. Soc.* **2002**, *124*, 3865.

(37) Johannissen, L. O.; Irebo, T.; Sjödin, M.; Johansson, O.; Hammarström, L. *J. Phys. Chem. B* **2009**, *113*, 16214.

(38) Klahr, B.; Gimenez, S.; Fabregat-Santiago, F.; Bisquert, J.; Hamann, T. W. *J. Am. Chem. Soc.* **2012**, *134*, 16693.

(39) Klahr, B.; Hamann, T. *J. Phys. Chem. C* **2014**, *118*, 10393.

(40) Dau, H.; Limberg, C.; Reier, T.; Risch, M.; Roggan, S.; Strasser, P. *ChemCatChem* **2010**, *2*, 724.

(41) Chen, J.; Li, Y.-F.; Sit, P.; Selloni, A. *J. Am. Chem. Soc.* **2013**, *135*, 18774.

(42) Li, Y.-F.; Liu, Z.-P.; Liu, L.; Gao, W. *J. Am. Chem. Soc.* **2010**, *132*, 13008.

(43) Le Formal, F.; Pastor, E.; Tilley, S. D.; Mesa, C. A.; Pendlebury, S. R.; Grätzel, M.; Durrant, J. R. *J. Am. Chem. Soc.* **2015**, *137*, 6629.

(44) Yamaguchi, A.; Inuzuka, R.; Takashima, T.; Hayashi, T.; Hashimoto, K.; Nakamura, R. *Nat. Commun.* **2014**, *5*, 4256.

DOI: 10.1021/jacs.5b12069
J. Am. Chem. Soc. 2016, 138, 2705−2711

(45) Kanan, M. W.; Nocera, D. G. *Science* **2008**, *321*, 1072.
(46) Kim, J. Y.; Jang, J.-W.; Youn, D. H.; Magesh, G.; Lee, J. S. *Adv. Eng. Mater.* **2014**, *4*, 1400476.
(47) Sawyer, D. T.; Sobkowiak, A.; Roberts, J. L. *Electrochemistry for Chemists*; Wiley-Interscience: New York, 1995.

DOI: 10.1021/jacs.5b12069
J. Am. Chem. Soc. 2016, 138, 2705−2711